JOURNAL OF SPACECRAFT AND ROCKETS
Vol. 34, No. 2, March–April 1997

Trajectory-Based Validation of the Shuttle Heating Environment

Dave Olynick* and Tim Tam*
NASA Ames Research Center, Moffett Field, California 94035-1000

Chemically reacting, three-dimensional, full Navier–Stokes calculations are generated around the shuttle orbiter and are compared with the STS-2 flight database at eight trajectory locations. Numerical estimates of quantities necessary for thermal protection system design, surface temperature and heating profiles, integrated heat load, bond-line temperatures, and thermal protection system thicknesses are compared with the STS-2 shuttle data. The effects of surface kinetics, turbulence, and grid resolution are investigated. It is concluded that trajectory-based thermal protection system sizing, the use of a Navier–Stokes flow solver combined with a conduction analysis applied over an entry trajectory, is a beneficial tool for future thermal protection system design. This conclusion is based on a reasonable agreement between the flight data and numerical predictions of surface heat transfer and temperature profiles, integrated heat loads and bond-line temperatures at most of the wind-side thermocouples. The effects of turbulent heating on thermal protection system design are illustrated. For future large entry vehicles, it is concluded that the prediction of turbulent transition will be a major driver in the thermal protection system design process. Finally, one potential payoff of using trajectory-based thermal protection system sizing, a reduction in thermal protection system mass, is illustrated.

Nomenclature

C_T	= heat transfer coefficient, W/m^2-K
c_p	= heat capacity of solid
c_s	= mass fraction for species s
D	= diffusion coefficient, m^2/s
E	= activation energy, K
h_s	= enthalpy of species s, m^2/s^2
K_w	= first-order reaction rate at wall, m/s
k	= Boltzmann constant, J/K
k_{solid}	= thermal conductivity of the solid
m_s	= mass of species s, kg
n_s	= number of species
$n, n+1$	= superscripts for time level
q_{cond}	= conductive heat flux, W/cm^2
q_{conv}	= total convective heat flux, W/cm^2
q_{ref}	= reference heat flux, W/cm^2
r	= numerical underrelaxation parameter
T_{rec}	= recovery temperature, K
T_{ref}	= reference temperature, K
T_w	= wall temperature, K
T_∞	= freestream temperature, K
α	= angle of attack
γ_s	= fraction of species s recombined on surface
ϵ	= surface emissivity
η	= normal direction component
κ	= thermal conductivity of gas, W/m-K
ρ	= mixture density, kg/m^3
σ	= Stefan–Boltzmann constant, W/cm^2-K^4

Introduction

TWO recent NASA initiatives, the X-33 and X-34 programs, are focused on development of inexpensive reusable launch vehicles (RLV). Currently, NASA funding and staffing levels are both declining. Nevertheless, the X-33 and X-34 programs have proceeded because the promise of cheaper access to space has been deemed a priority that is critical to meeting the nation's future space exploration needs.

A few goals of the X-33 and X-34 programs are to reduce current payload to orbit costs by an order of magnitude and to foster development of a private space launch industry. The X-33 vehicle is envisioned as a fully reusable, single-stage-to-orbit rocket. The vehicle will serve as a technology demonstrator for a RLV, which will be capable of boosting a payload of up to 25,000 lb into a low Earth orbit, return to Earth, and be ready to launch again in a week. A typical mission for an X-33 type RLV will be resupply of the international space station. Currently, the X-34 vehicle concept is envisioned as a technology demonstrator for a winged rocket, which will launch from a subsonic aircraft, deliver a satellite and expendable booster into a low Earth orbit, and then return and land on a runway.

The X-33 and X-34 programs are industry-led teaming efforts between NASA and industry. A few vehicle concepts that have been considered in the X-33 program are winged bodies, lifting bodies, and vertical takeoff and landers. Because one purpose of the programs is to foster a private launch business and industry is providing significant amounts of its own resources, the vehicle conceptual designs are being driven by factors that will maximize the potential for return on investment such as minimizing operation, maintenance, and acquisition costs.

A subsystem that is of critical importance to the RLV program is the thermal protection system (TPS). A TPS is needed to protect the structure of the vehicle during ascent and re-entry. Most of the materials that will be used in fabrication of the RLV structure, such as carbon composites or aluminum, can withstand temperatures of only about 350°F and still maintain reusability. These temperatures are greatly exceeded during RLV flight conditions. Further, from shuttle experience, the TPS has been identified as an area where large improvements can be made in operations and maintenance costs. Finally, the TPS mass fraction is large enough to be targeted for potential weight savings.

TPS components are designed so that maximum structural and TPS reuse temperature limits are not exceeded during entry. Exceeding maximum reuse temperatures during flight operations can increase vehicle life cycle costs through increased inspection, maintenance, and replacement costs associated with the TPS and structure. Conversely, if the TPS is overdesigned, then the extra weight reduces the potential payload size, increases the payload costs because each flight carries less payload, and increases operation and maintenance costs associated with the additional TPS. Thus, a TPS

Received July 16, 1996; revision received Nov. 27, 1996; accepted for publication Dec. 6, 1996.

*Research Scientist, Reacting Flow Environments Branch, MS 230–2. Member AIAA.

design is sought that minimizes operational costs, weight, and risk. To design a TPS, accurate characterization of the aerothermal environment during flight is needed. In particular, maximum surface temperatures, total integrated heat loads, and aerodynamic load data are required. The maximum surface temperatures and aerodynamic load data are required for TPS material selection. The heat transfer as a function of time, which is characterized by the integrated heat load, is needed to size the TPS.

The needed aerothermodynamic quantities for the TPS design of a re-entry vehicle are usually obtained by a combination of experimental and numerical simulations.[1] An important issue that arises in development of an aerothermal TPS design database is the validity and accuracy of extrapolating ground-based experimental, numerical, and existing flight data to actual design conditions. For example, most of the X-33 concepts are envisioned as subscale and suborbital technology demonstrators for a larger, orbital RLV. The expected heat loads for the X-33 are much less than those predicted for a full-scale vehicle. Further, transition to turbulence, which can greatly increase the integrated heat load, is a nonlinear function of the vehicle's dimensions. Thus, it has been questioned whether the aerothermal database developed for X-33 will be applicable to the larger RLV. Uncertainties in the TPS design database lead to increased design margins. Increased TPS design margins, which also affect the margins of associated subsystems such as the structure, cost money.

The focus of this paper is to use high-fidelity numerical simulation to address some of the uncertainties associated with generating a TPS design database. The approach, which is called trajectory-based TPS sizing, is to use a three-dimensional, chemically reacting, Navier–Stokes code in conjunction with a conduction program to predict integrated heat loads, maximum surface temperatures, bond-line temperatures, and TPS thicknesses for a RLV. This methodology has been described and demonstrated for a number of RLV concepts employing ceramic TPS.[2–5] The goal of this paper is to assess the validity and accuracy of the methodology through comparison with the STS-2 flight database.[6]

For this study, the STS-2 entry trajectory was discretized at eight locations ranging from Mach 26.3 at 79.3 km to Mach 6.04 at 38.9 km. The numerically predicted convective heat transfer vs time curves were compared with the STS-2 flight data at 11 thermocouple locations over the vehicle's surface. Included in the comparisons are the effects of two surface kinetic models, the component of heating due to catalytic recombination, laminar vs turbulent flow, and a grid resolution study at five points. The heat transfer vs time curves were used to generate integrated heat loads, which were compared with the flight data. Further, the heat transfer vs time curves using both the laminar and turbulent calculations were used as input to a one-dimensional conduction solver to generate surface and bond-line temperature profiles. The surface temperature profiles were compared with flight data at 11 thermocouple locations and bond-line data comparisons were made at 7 locations. Finally, at each thermocouple location using the numerical heat transfer profiles, the TPS was resized so that the temperature at the TPS–structural interface (bond line) was within 1 K of the maximum reuse temperature for the structure, which is 450 K for aluminum. These new thicknesses were compared with the tile thicknesses used on the flight.

In a previous comparison with the shuttle STS-2 flight data,[7] calculations at three trajectory points were performed with the LAURA code.[8] Numerical and flight heat transfer data were compared at numerous surface locations. A reasonable agreement was obtained with the flight data. These three trajectory points and five others were used in the present study. Although not compared in this work, the fidelity of the heat transfer results generated using LAURA and the results presented in this study is similar.

Procedure

Fluid Flow Governing Equations

In this study, a set of governing equations were chosen that are appropriate for a shuttle-like entry heating environment.[7,9] A set of the Navier–Stokes equations employing finite-rate chemistry were solved that included five species equations (N_2, O_2, NO, N, O), three momentum equations, and one energy equation. The flow was assumed to be in thermal equilibrium. In the thermal boundary layer near the surface, the internal modes are near equilibrium and most of the ions are recombined. Thus, thermal nonequilibrium and ionization have a minimal impact on the predicted heat transfer rate. The adequacy of these assumptions for predicting surface heat transfer is discussed in Ref. 5.

The multispecies Navier–stokes equations described earlier were solved by using the finite-volume general aerothermodynamic simulation program (GASP) version 2.2 flow solver.[10,11] The implementation of the GASP code allows the user to choose from a large number of numerical modeling and time integration strategies. For calculating blunt body, re-entry type flow problems,[2–5] the following implementation of the code has been shown to produce good numerical heat-transfer predictions, reasonable convergence, and excellent robustness.

The equations were marched in time to steady state by using an implicit two-factor approximate factorization scheme in the cross-flow planes and employing underrelaxation in the streamwise direction. The upwind fluxes were modeled with a Van Leer formulation. A first-order scheme was used in the coordinate directions along and around the body. Normal to the body, the scheme was extended to the third order by a monotone upstream-centered scheme for conservation laws variable extrapolation.[12] The viscous fluxes were approximated by using central differences. The finite rate chemistry was modeled by using Park's reaction rates.[13]

The various transport properties were calculated with Wilkes semiempirical mixing rule[14] with curve fits for the species viscosities given by Blottner et al.[15] and a constant Schmidt number with Fick's law for the mass diffusion. For the fully turbulent flow calculation, an eddy viscosity was computed algebraically according to Baldwin–Lomax.[16]

Boundary Conditions and Material Properties

Accurate modeling of the fluid–surface interface for a re-entry vehicle requires knowledge of the thermal protection materials utilized in the heatshield and their associated properties. The major TPS materials of the Columbia orbiter for the STS-2 flight consisted of LI-900 and LI-2200 tiles, felt reusable surface insulation (FRSI), and reinforced carbon-carbon (RCC). The LI-900 and LI-2200 tiles were used on surfaces with estimated temperatures between 644 and 1589 K with LI-2200 used for areas with the highest heat loads. High-temperature resuable surface insulation (HRSI) refers to black, reaction-cured glass (RCG)-coated LI-900 or LI-2200 tiles. Low-temperature resuable surface insulation (LRSI) refers to white-coated LI-900 tiles. FRSI is used on the leeside surfaces and RCC is used for the nosecap and wing leading edges.[17]

Most of the surface temperature data from flight were obtained from thermocouple plugs embedded in LI-900 and LI-2200 tiles under the RCG coating. A few locations on the surface with FRSI contained thermocouples. No thermocouples were embedded in the RCC. The thermocouple data were used to generate surface temperatures and predict heat transfer rates during the flight.[6]

Shuttle TPS materials have various densities, thermal conductivities, and surface emissivities and catalysis. These properties are needed to accurately model the fluid–surface interface. The tiles were coated with a borosilicate glass compound called RCG,[18] which has been experimentally characterized. RCC employs surface coatings that are similar in composition to RCG. Thus, RCC surface properties were assumed to be equal to those of RCG. Finally, the FRSI surface catalysis is not as well known as the tiles or RCC. In this study, the FRSI surface properties were assumed equal to those of the tiles. On STS-2, FRSI was used only on the leeside areas exposed to the least heating. None of the thermocouple measurements used for comparisons in this work were at surface locations using FRSI.

TPS surface and in-depth properties are needed when modeling the mass and energy balances at the fluid–surface interface. The surface energy balance is given as[19]

$$\kappa \frac{\partial T}{\partial \eta} + \sum_{s}^{ns} \left(\rho D h_s \frac{\partial c_s}{\partial \eta} \right) = \sigma \epsilon T_w^4 + q_{\text{cond}} \qquad (1)$$

In this study, the q_{cond} term is assumed to be zero when calculating the heat transfer from the fluid to the surface. The impact of this assumption is discussed in the following section. A constant emissivity ϵ of 0.85, which does not vary with temperature, is used for all the materials in this work. This value is based on the measured RCG surface emissivity.[20] The emissivity value for RCC for the flight conditions considered in this study is slightly lower (between 0.85 and 0.81) (Ref. 21).

The surface catalysis was modeled by using first-order reaction rates. Thus, the mass flux at the wall can be related to the rate of diffusion toward the surface as

$$\left(\rho D \frac{\partial c_s}{\partial \eta}\right)_w = (\rho_s K_s)_w = \gamma_s \sqrt{\frac{kT_w}{2\pi m_s}} \tag{2}$$

where γ_s is curve fit as a function of temperature as

$$\gamma_s = C \exp^{-E/T_w} \tag{3}$$

Curve fits for γ_s of this form for RCG are given in Refs. 22 and 23. The curve fits were obtained experimentally with testing and measurements performed in an arc jet. Two sets of RCG kinetics were used in this study. In this work, the curve fits from Ref. 22 are denoted by old RCG kinetics and the values from Ref. 23 as new RCG kinetics.

Equations (1) and (2) are solved numerically in the following manner. Equation (2) is discretized as

$$\frac{(c_s)_1 - (c_s)_w}{\Delta\eta} = (c_s K_s)_w \tag{4}$$

where $\Delta\eta$ is the ratio of the grid cell volume to wall surface area, which is the appropriate metric in a finite volume formulation. The mass fractions of $(c_O)_w$ and $(c_N)_w$ are determined from Eq. (4) using T_w, $(c_O)_1$, and $(c_N)_1$ at the current time level. Then, the mass fractions of N_2 and O_2 are determined from the law of mass action. Next, the new mass fractions are substituted into the left-hand side of Eq. (1) and a total convective heat flux q_{conv} is calculated. Finally, the surface temperature is updated by underrelaxation as[7]

$$T_w^{n+1} = r\left(\frac{q_{\text{conv}}}{\epsilon\sigma}\right)^{0.25} + (1-r)T_w^n \tag{5}$$

where a value of $r = 0.01-0.02$ is used.

In-Depth Conduction

The conduction into the solid is given by

$$\rho c_p \frac{\partial T}{\partial t} = \frac{\partial}{\partial \eta}\left(\kappa_{\text{solid}} \frac{\partial T}{\partial \eta}\right) = \frac{\partial q_{\text{cond}}}{\partial \eta} \tag{6}$$

Solutions to this equation were generated with the OMLITS[24] code. The conduction term, q_{cond} in Eq. (1), is a function of time. Because the amount of conduction affects the convective heat transfer through the energy balance equation, the fluid and solid equations should be solved in a coupled manner.

In Ref. 24, it was determined that coupling conduction directly into the flow calculation was unnecessary for a nonablating, ceramic TPS. The procedure developed in Ref. 24 is as follows. In the flow calculation, Eq. (1) is solved with $q_{\text{cond}} = 0$. The heat transfer from the flow solver neglecting conduction is written in terms of the heat-transfer coefficient as

$$q_{\text{conv}} = \kappa \frac{\partial T}{\partial \eta} + \sum_s^{ns}\left(\rho D h_s \frac{\partial c_s}{\partial \eta}\right) = C_T(T_{\text{rec}} - T_w) \tag{7}$$

In OMLITS, a new wall temperature T_w accounting for conduction is generated by the following surface energy balance equation

$$C_T(T_{\text{rec}} - T_w) = \sigma\epsilon T_w^4 + q_{\text{cond}} \tag{8}$$

The wall temperature generated by the previous equation could be used in the computational fluid dynamics (CFD) solution as a new boundary condition and the procedure repeated until convergence is obtained. It was concluded that this procedure was unnecessary because after only one iteration a wall temperature was generated that was within 3% or less of the value from an iteratively coupled flow and conduction solution. This result remained valid for conductive heat fluxes that were as high as 50% of the convective heat flux. This procedure, one iteration between the flow solver and OMLITS, is used in the present work.

Results

The major objective of this study was to assess the accuracy and fidelity of a numerical TPS sizing algorithm that employs the Navier–Stokes equations to model the fluid and a one-dimensional conduction code to model the TPS. In particular, the assessment of ceramic TPS applied to a RLV was of prime interest. The best set of experimental data available that characterize a RLV entry are the thermocouple data from the early shuttle flights. Eight flight conditions chosen for this study are given in Table 1. The locations of these points on the STS-2 re-entry trajectory are shown in Fig. 1. The points at 75,620, 75,950, and 76,130 s were selected to compare with previous solutions obtained by the LAURA code.[7] The remaining points were selected to capture the shape of the heat-transfer pulse. It is assumed that the heat transfer is negligible at the 75,140 and 76,490 conditions. Thus, the length of the heat pulse is 1350 s.

The STS-2 thermocouple data showed that the 76,240 s, Mach 9.57, trajectory point was just before turbulent transition at a number of thermocouple locations; for the 76,390 s, Mach 6.0 trajectory point, the flow appears to be fully turbulent over the entire vehicle. In general, the flight conditions at which turbulent transition occurs are not well known or easily predicted. For the shuttle, it has occurred for Mach numbers ranging from 5.8 to 17.5 and freestream Reynolds numbers from 2.5×10^6 and 1.3×10^7 (Ref. 25). It is suspected that this variation is a function of the trajectory and the orbiter TPS conditions such as steps and gaps, which vary from flight to flight and orbiter to orbiter. On one flight, it is believed that a tile gap filler protruding into the flow caused an early asymmetric turbulent transition. Once transition occurs, it quickly moves up the vehicle; flight data indicate that the time for the transition front to move up the windward surface is usually on the order of 1 min. Because the integrated heat load greatly increases as transition nears the peak heating location in the trajectory, the prediction of turbulent heating significantly impacts the sizing of the TPS. For this reason, the trajectory of the shuttle was shaped to delay the onset of transition. Thus, the fully turbulent calculations at the Mach 9.57 and 6.0 conditions have two purposes: first, to determine how well a simple

Table 1 Shuttle STS-2 flight conditions

Time, s	Altitude, km	Velocity, km/s	Density, kg/m^3	T_∞, K	Mach	α, deg
75,350	79.3	7.439	1.82×10^{-5}	200.1	26.23	39.4
75,420	76.1	7.353	3.18×10^{-5}	198.2	26.06	40.2
75,620	72.4	6.920	5.75×10^{-5}	202.0	24.3	39.4
75,790	69.2	6.389	9.05×10^{-5}	215.3	21.7	38.8
75,950	64.4	5.617	1.626×10^{-4}	240.6	18.07	41.2
76,130	54.8	4.168	5.330×10^{-4}	261.6	12.86	39.7
76,240	48.7	3.100	1.164×10^{-3}	255.4	9.57	36.6
76,390	38.9	1.897	4.599×10^{-3}	245.9	6.038	24.7

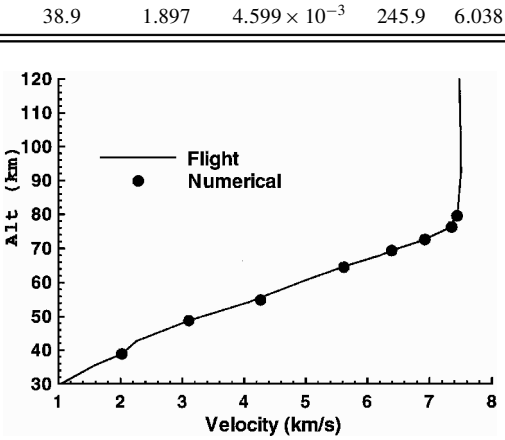

Fig. 1 Trajectory points for flow calculations: STS-2 flight trajectory.

Table 2 Numerical calculation matrix

Run	Time, s	Gas model	Flow type	Grid	Kinetics
1	75,350	5 species	laminar	coarse	new RCG
2	75,350	5 species	laminar	coarse	old RCG
3	75,350	5 species	laminar	fine	old RCG
4	75,420	5 species	laminar	coarse	new RCG
5	75,420	5 species	laminar	coarse	old RCG
6	75,420	5 species	laminar	fine	old RCG
7	75,620	5 species	laminar	coarse	new RCG
8	75,620	5 species	laminar	coarse	old RCG
9	75,790	5 species	laminar	coarse	new RCG
10	75,790	5 species	laminar	coarse	old RCG
11	75,950	5 species	laminar	coarse	new RCG
12	75,950	5 species	laminar	coarse	old RCG
13	75,950	5 species	laminar	fine	old RCG
14	76,130	5 species	laminar	coarse	new RCG
15	76,130	5 species	laminar	coarse	old RCG
16	76,130	5 species	laminar	fine	old RCG
17	76,240	5 species	laminar	coarse	new RCG
18	76,240	5 species	laminar	coarse	old RCG
19	76,240	5 species	laminar	fine	old RCG
20	76,240	5 species	turbulent	fine	new RCG
21	76,390	perfect gas	laminar	coarse	none
22	76,390	perfect gas	turbulent	coarse	none

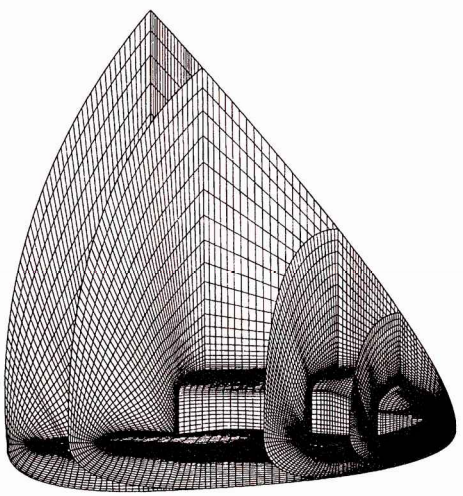

Fig. 2 Flow grid used for shuttle calculations, 80 × 75 × 51.

algebraic turbulence model such as Baldwin–Lomax predicts turbulent heating levels; second, because the Mach 9.6 trajectory point is before the onset of transition at most of the thermocouple locations, to determine the sensitivity of the TPS thicknesses relative to the prediction of transition.

Figure 2 is a plot of a typical grid used for the flow calculations in this study. The grid contains 80 points along the body, 75 in the circumferential direction and 51 normal to the surface. In this work, the vertical stabilizer was removed to simplify the CFD computation. Further, the fine details of the surface such as tiles gaps and seals were not captured. The flow was assumed to be symmetric about each half of the vehicle; small side-slip angles in the flight data have been ignored. To determine normal grid convergence, calculations were run at five flow conditions with the number of normal grid points doubled. Further, grid convergence studies at the Mach 18 and 24 flight conditions are described in Ref. 26. In this work, coarse refers to calculations on the 80 × 75 × 51 grid and fine refers to calculations on the 80 × 75 × 101 grid.

In this study, 22 three-dimensional Navier–Stokes flow solutions are generated. These calculations are summarized in Table 2. New and old RCG refer to experimentally determined catalytic efficiencies, γ_s in Eq. (3). Turbulent refers to fully turbulent calculations with a Baldwin–Lomax model. The chemical model, five species, consists of N_2, O_2, NO, O, and N. For comparison with the flight thermocouple data, these runs are divided into four trajectory groups, old RCG, new RCG, turbulent, and fine. The old RCG group, runs 2, 5, 8, 10, 12, 15, 19, and 21, are laminar calculations using the old RCG kinetics on the coarse grids. The new RCG group, runs

Table 3 Comparison of integrated heat loads

		Integrated reference heat load, s				
Measurement	Material	STS-2	Old RCG	New RCG	Catalytic	Turbulent
99,341	HRSI	535.6	577.1	546.4	146.0	574.6
99,337	LRSI	44.0	41.1	41.6	0.934	51.0
79,876	HRSI	53.5	57.9	57.9	1.43	69.4
79,813	LRSI	17.4	14.7	15.0	0.22	16.7
99,381	HRSI	211.0	224.4	211.0	19.4	248.3
99,201	HRSI	304.8	317.9	309.0	20.9	323.3
79,901	LRSI	27.1	28.4	28.6	0.48	32.0
79,622	LRSI	20.3	33.2	33.5	0.17	36.8
99,171	HRSI	235.0	200.3	191.8	13.1	243.0
99,761	LRSI	169.6	167.9	161.5	10.8	203.9
99,191	HRSI	271.7	244.1	233.8	19.7	266.6

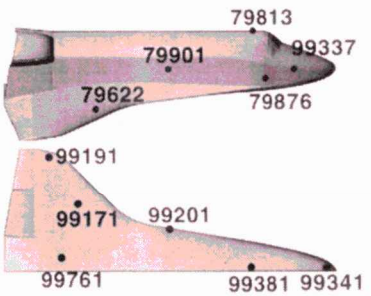

Fig. 3 Thermocouple locations for data comparisons.

1, 4, 7, 9, 11, 14, 17, and 22, are laminar calculations using new RCG kinetics on the coarse grids. The turbulent group, runs 1, 4, 7, 9, 11, 14, 20, and 22, are laminar calculations before 76,240 s and fully turbulent for the 76,240 and 76,390 conditions. The new RCG kinetics are employed for this group. Finally, the fine group, runs 3, 6, 13, 16, and 19, are laminar calculations using the old RCG kinetics on the fine grids. The thermocouple locations on the shuttle body for the data comparisons with the various groups are shown in Fig. 3 and the material type for each thermocouple is shown in Table 3. The 99– are points where both surface and bond-line data are available. For the 79– points, surface data only are available.

Comparisons of Heat Transfer Profiles and Integrated Heat Load

Figures 4–14 are plots comparing flight-derived and numerical heat transfer predictions vs time at the various surface locations for the four trajectory groups (see Fig. 3 for approximate surface location for each measurement). Included are the magnitude of the numerically predicted catalytic heating. The flight data are represented along the trajectory at 100-s intervals starting at 75,040 s except near transition, where additional points were included. (The authors did not have access to the data on computer and had to generate the plots from tables in the data book.) The flight data book contains data at 10-s intervals, and plots in the data book employing all of the data are less smooth. The estimated error for the flight heat-transfer data is tabulated in Ref. 6; the magnitude of the estimated error is usually between 5 and 8% of the total convective heat transfer.

Overall, the numerical prediction of the magnitude and shape of the heat-transfer profiles are in reasonable agreement with the flight data. The best comparisons are obtained for the windside thermocouples in Figs. 5, 6, 8, 9, and 12–14; both the shape and the magnitude of the heat transfer profiles are in good agreement with the flight data. In Figs. 4, 7, 10, and 11, the comparisons are not as good.

For the thermocouple shown in Fig. 4, the numerical heat transfer is significantly above the flight data at the Mach 24.3 and Mach 21.7 conditions. It is likely that grid effects account for some of the difference. Because of the high shock curvature and large entropy gradients near the nose, it has been shown that the heat transfer is very sensitive to grid topology and grid density.[26] Also, the modeling of thermal and chemical nonequilibrium, which are strongly coupled to surface heat transfer through catalysis, causes some of the difference. In Fig. 8, which is farther from the nose on the windward centerline, the shock curvature and nonequilibrium effects are less important and better agreement with the flight data is obtained.

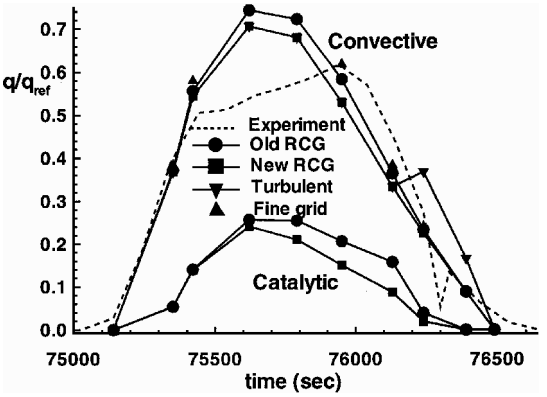

Fig. 4 Comparison of numerical and experimental heating distributions for STS-2, windside centerline: thermocouple measurement 99,341.

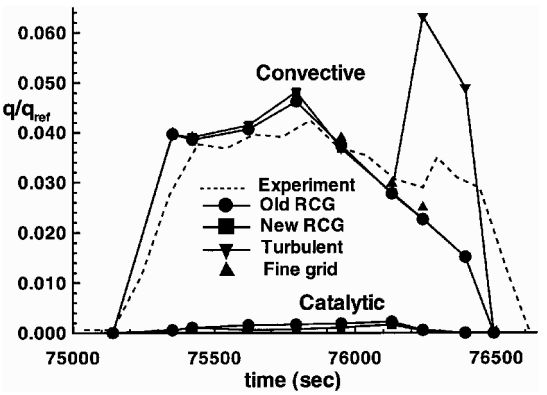

Fig. 5 Comparison of numerical and experimental heating distributions for STS-2, side ahead of cockpit: thermocouple measurement 99,337.

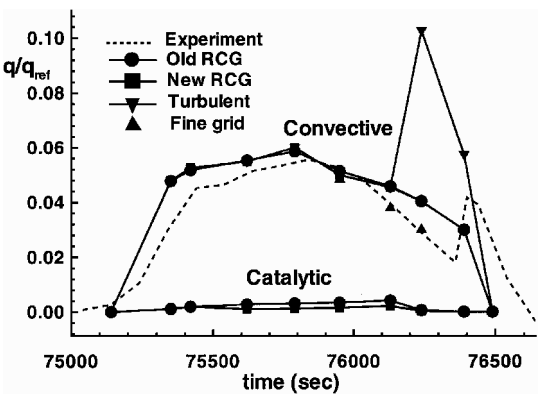

Fig. 6 Comparison of numerical and experimental heating distributions for STS-2, side below cockpit: thermocouple measurement 79,876.

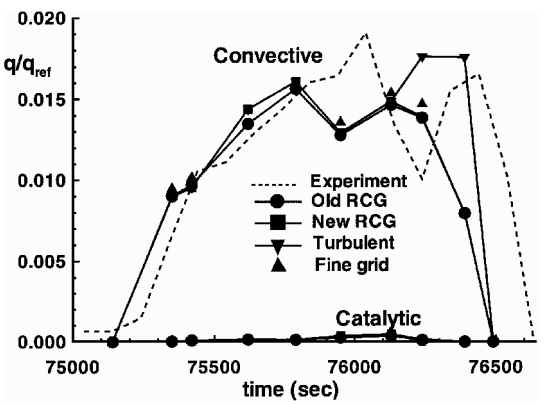

Fig. 7 Comparison of numerical and experimental heating distributions for STS-2, leeside centerline: thermocouple measurement 79,813.

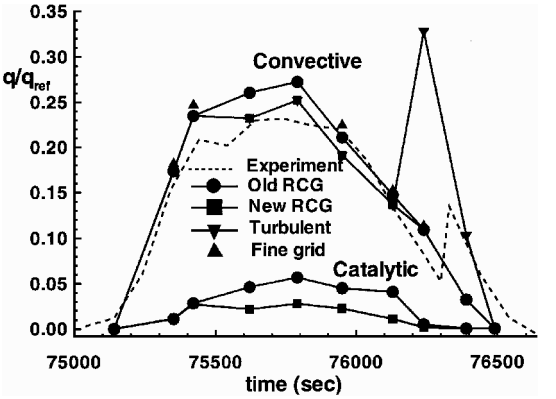

Fig. 8 Comparison of numerical and experimental heating distributions for STS-2, windside centerline: thermocouple measurement 99,381.

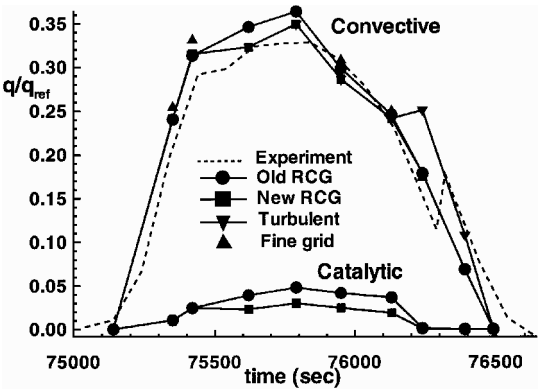

Fig. 9 Comparison of numerical and experimental heating distributions for STS-2, chine leading edge: thermocouple measurement 99,201.

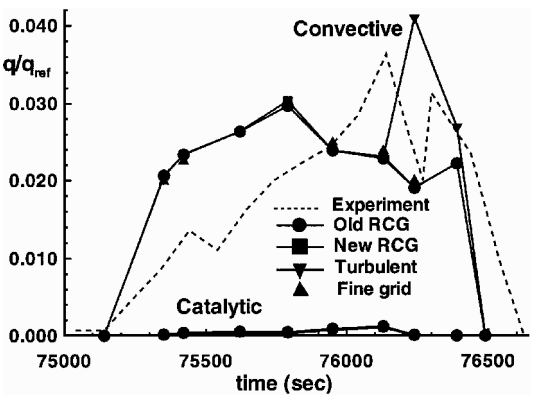

Fig. 10 Comparison of numerical and experimental heating distributions for STS-2, side, midcargo bay: thermocouple measurement 79,901.

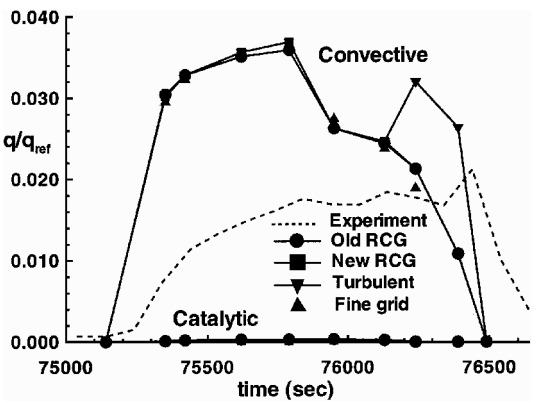

Fig. 11 Comparison of numerical and experimental heating distributions for STS-2, top of wing, near midspan leading edge: thermocouple measurement 79,622.

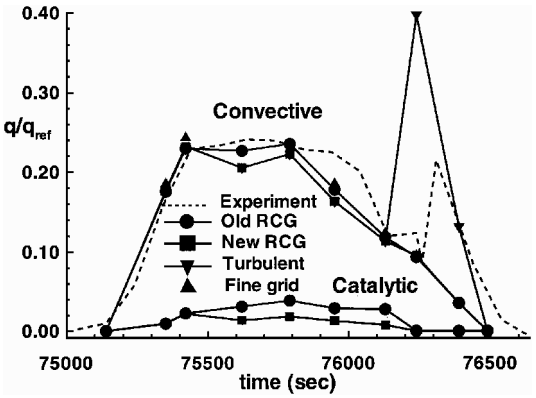

Fig. 12 Comparison of numerical and experimental heating distributions for STS-2, windside, midwing: thermocouple measurement 99,171.

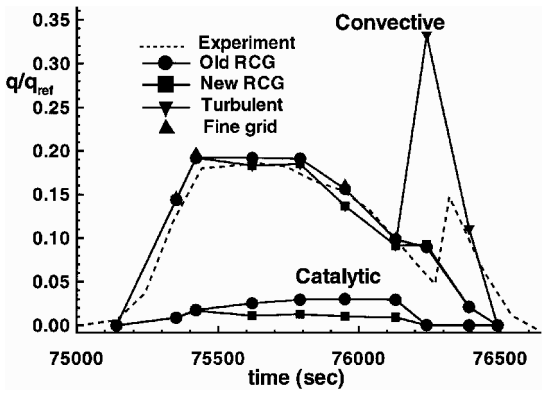

Fig. 13 Comparison of numerical and experimental heating distributions for STS-2, near windside centerline, 80% length: thermocouple measurement 99,761.

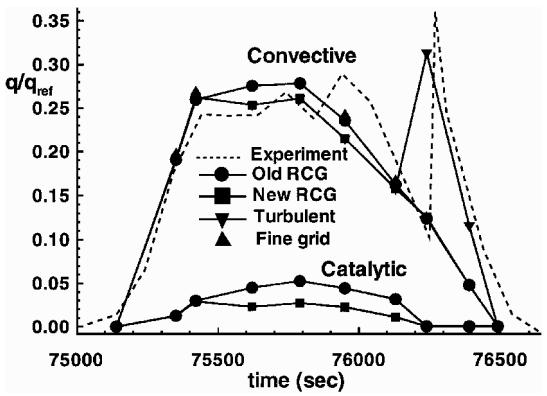

Fig. 14 Comparison of numerical and experimental heating distributions for STS-2, near wing tip: thermocouple measurement 99,191.

In Figs. 7, 10, and 11, which are on the leeside centerline, below the cargo bay hinge line and on top of the wing, it is believed that the complex nature of the flowfield combined with inadequate grid resolution causes the differences between the numerical and flight heat transfer. In Figs. 7 and 11, the flow is expanding; there are shock-on-shock interactions and possibly flow separation. In Fig. 10, there is a large vortex emanating near the nose that scrubs the side of the vehicle and eventually impacts the orbital maneuvering system pods. The comparisons were not improved by increasing the normal grid resolution as shown by the fine-grid calculations. To resolve some of these flow features, grid resolution is required in the cross-flow direction.

The numerical predictions of the heat transfer using the new and old RCG kinetics were similar. The magnitude of the total heating with the new RCG kinetics was slightly lower, but the levels were in better agreement with the flight data. The fraction of the surface heat transfer resulting from catalysis varies from as high 33% near the nose to 10–20% on windside portions of the vehicle; it is neglible on leeside portions of vehicle.

In general, the five calculations on the fine grids show slightly higher heating rates relative to calculations on the coarse grids. Further, as noted previously, discrepancies between the numerical and flight heat-transfer predictions on the leeside centerline, top of the wing and below the cargo bay hinge line, were not improved by increasing the grid resolution normal to the surface. Thus, it is concluded that 50 points normal to the surface used on the coarse grids adequately resolved the viscous gradients normal to the surface necessary for calculation of the heat transfer.

Predictions of the surface heating, assuming fully turbulent flow at Mach 9.6, are usually much higher than the flight data. Because the Mach 9.6 conditions were before transition, higher heating levels were expected. In Fig. 14, where the Mach 9.6 conditions are just before transition, the turbulent heating prediction agrees well with the flight data. For the thermocouple locations where the Mach 6.0 conditions are clearly after transition (Figs. 4, 8–10, and 12–14), the turbulent heating predictions are in good agreement with the flight data. It is concluded from this comparison that a simple algebraic Baldwin–Lomax model is at least adequate for predicting the qualitative effects of turbulent heating.

As previously discussed, an accurate estimate of the heat load is needed for TPS sizing. A major objective of this study was to assess the applicability of a Navier–Stokes methodology for predicting integrated heat loads. Table 3 contains a comparison of the integrated reference heat load at each thermocouple for the STS-2, old RCG, new RCG, and turbulent groups. The heat load is normalized by using q_{ref}. The catalytic values are the fraction of the heating from surface catalysis for the new RCG group. When new RCG and the STS-2 values were compared, the errors varied from an overprediction of 65% for 79,622 to an underprediction of 18% for 99,171 to almost no error for 99,381. Moreover, a good comparison with the heat load was obtained at locations where the shape of the numerical heat-transfer profile did not agree with the flight data. For example, for 99,341 and 79,901 in Figs. 4 and 10, the heat transfer is overpredicted early in the trajectory but underpredicted later in the trajectory; these errors cancel and the new RCG values for the heat load compare well with the flight data.

At 99,341, which is near the nose, the catalytic heat load predicted is about 30% of the total heat load; this percentage is the maximum value for the thermocouples shown in this study. Further, the magnitude and percentage of the catalytic heat load are much less than at the other thermocouple locations. Nevertheless, the effects of the catalytic heating are an important design driver because the TPS materials on the nose and wing leading edges are close to their maximum reuse temperatures during entry. This factor limits the types of entry trajectories and mission scenarios for the shuttle. Thus, a decrease in the catalytic heat load or an increase in the maximum reuse temperature of the nose and leading edge TPS materials would increase the possible entry trajectories and the operational envelope of the shuttle.

For the windside thermocouples 99,381, 99,201, 99,171, 99,191, and 99,761, the heat load predicted for the turbulent group is 20–25% higher than for the new RCG group. For these thermocouples, the Mach 9.6 trajectory point is about 70–90 s before the peak turbulent heating value. At the thermocouple locations where the flow is still laminar at Mach 9.6, the numerical turbulent heating values are 3–4 times higher than the flight data, which is a reasonable enhancement. Thus, given the shape of the heat-transfer profile, which steeply drops after peak heating, it is concluded that the choice of a transition criterion will be a major driver in the TPS design of future entry vehicles. For an overly conservative criterion, heat load and TPS thicknesses will be greatly overestimated. Given the inconsistency of transition observed for the shuttle,[25] this topic will be an area of much concern for the TPS design of a RLV.

After reviewing the comparisons of heat-transfer profiles and integrated heat loads with the flight data shown in this study—more surface locations have been examined but are not included because of space limitations—the following conclusions were made. For the windside thermocouples, where the flow structure is relatively simple, the present methodology is adequate for predicting integrated

heat loads. This conclusion is important because most of the TPS mass is on the windside of the vehicle. Further, it is believed that the fidelity of the methodology will improve as more trajectory points are included. For areas where the flow structure is more complex, such as along the cargo bay hinge line or on top of the wing, a higher fidelity calculation will be required to resolve the heat transfer. However, because the calculations tend to be conservative and the total heat load is small in these areas, using these calculations to size the TPS will have only a minimal impact on the overall TPS mass. Thus, relative to the design of the TPS, higher fidelity calculations are not necessary.

Comparisons of Surface and Bond-Line Temperatures

In this section, two other quantities important for TPS design, surface and bond-line temperatures, are examined. The maximum surface temperature during entry is needed for TPS material selection and the maximum bond-line temperature is an important parameter for TPS sizing. The heat-transfer profiles described in the prior section are used as input for a one-dimensional conduction code. The output from the conduction code, surface and bond-line temperatures, are compared with the flight data. Figures 15–25 show a comparison between numerical and flight surface temperatures vs time, where the surface temperatures are scaled by a reference value. For 99– thermocouples, a comparison between the numerical and flight bond-line temperatures is presented; the scale for the referenced bond-line temperatures is shown on the second y axis. The numerical results are for the new RCG and turbulent groups. Finally, the time scale is altered from the previous figures; the zero on the time axis in Figs. 15–25 corresponds to 75,040 s in Figs. 4–14.

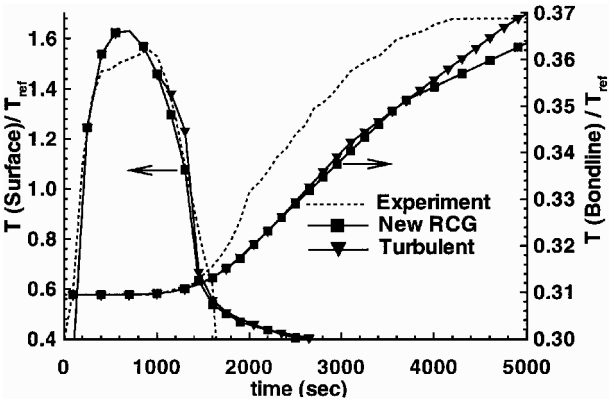

Fig. 15 Comparison of numerical and experimental surface and bond-line temperature distributions for STS-2, windside centerline: thermocouple measurement 99,341.

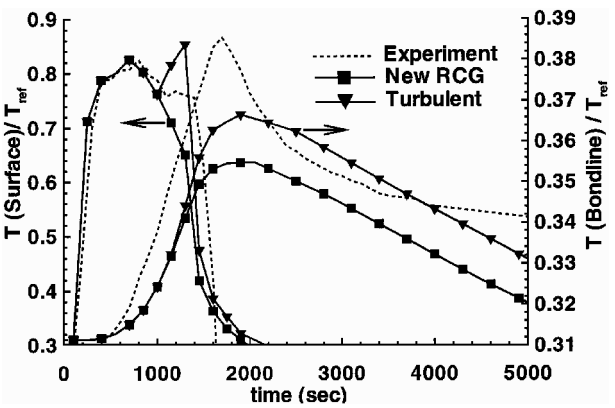

Fig. 16 Comparison of numerical and experimental surface and bond-line temperature distributions for STS-2, side ahead of cockpit: thermocouple measurement 99,337.

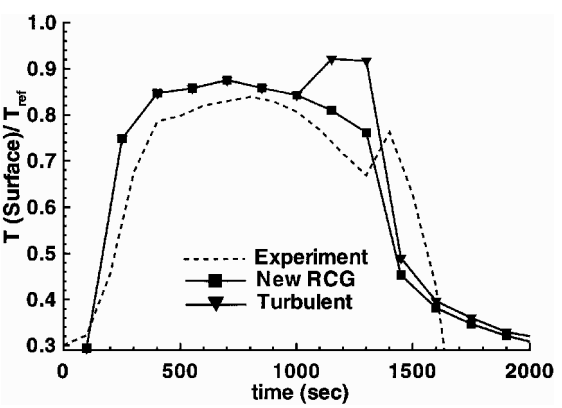

Fig. 17 Comparison of numerical and experimental surface temperature distributions for STS-2, side below cockpit: thermocouple measurement 79,876.

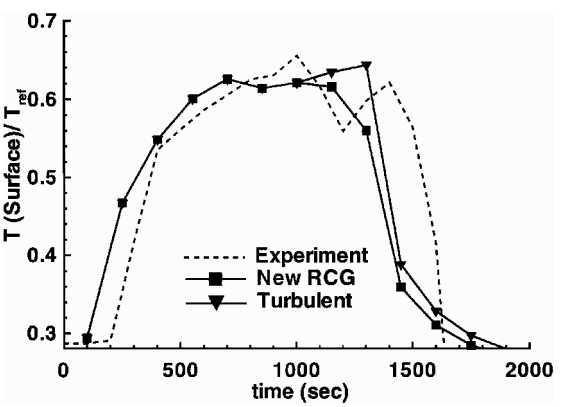

Fig. 18 Comparison of numerical and experimental surface temperature distributions for STS-2, leeside centerline: thermocouple measurement 79,813.

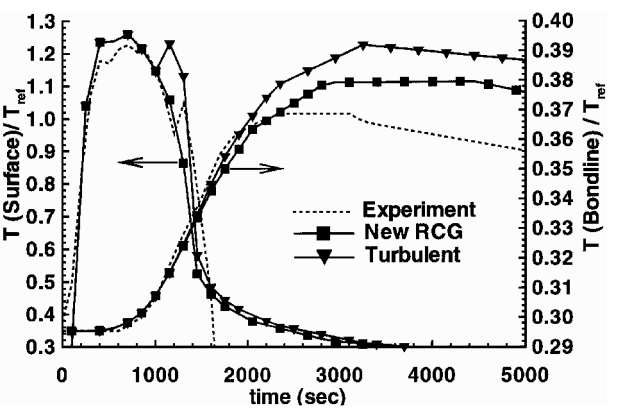

Fig. 19 Comparison of numerical and experimental surface and bond-line temperature distributions for STS-2, windside centerline: thermocouple measurement 99,381.

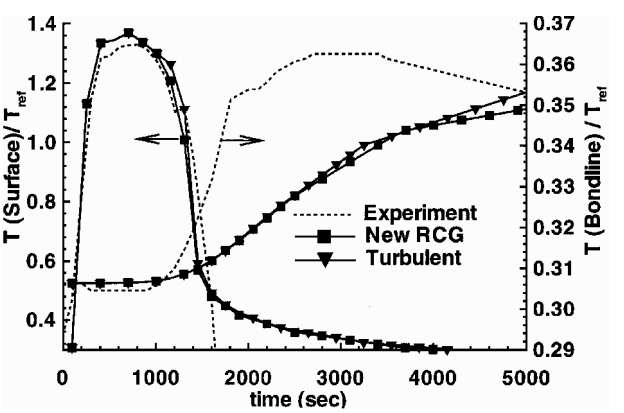

Fig. 20 Comparison of numerical and experimental surface and bond-line temperature distributions for STS-2, chine leading edge: thermocouple measurement 99,201.

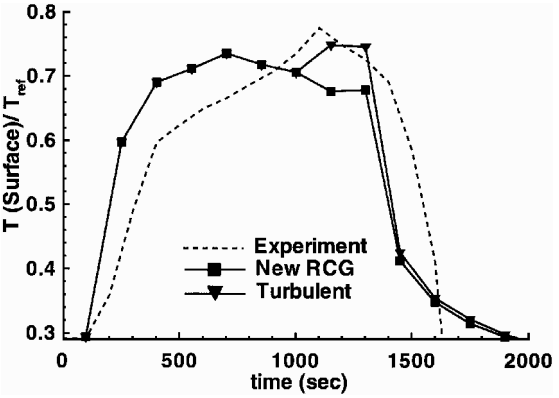

Fig. 21 Comparison of numerical and experimental surface temperature distributions for STS-2, side, midcargo bay: thermocouple measurement 79,901.

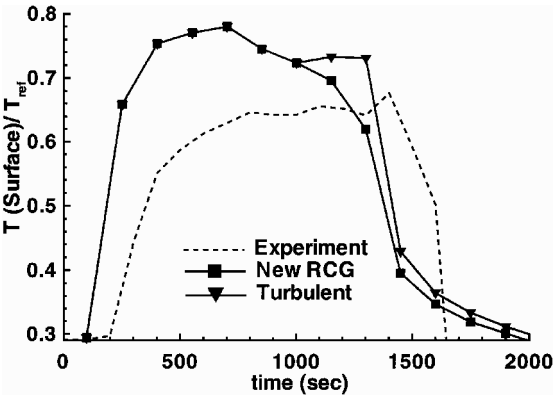

Fig. 22 Comparison of numerical and experimental surface temperature distributions for STS-2, top of wing, near midspan leading edge: thermocouple measurement 79,622.

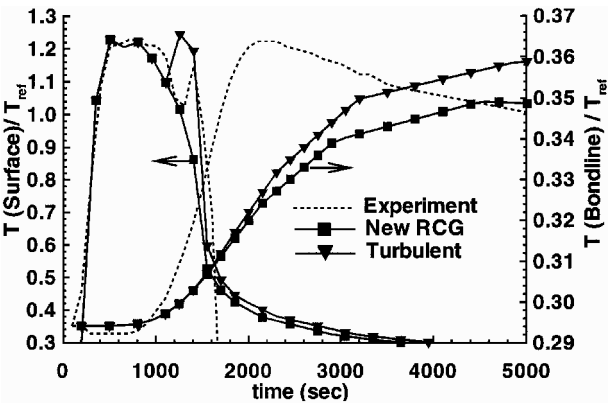

Fig. 23 Comparison of numerical and experimental surface and bondline temperature distributions for STS-2, windside, midwing: thermocouple measurement 99,171.

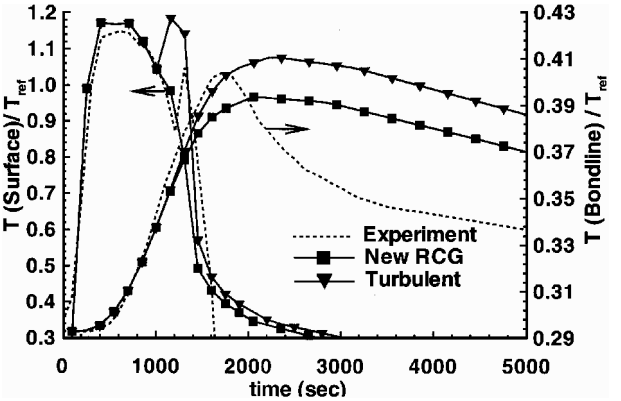

Fig. 24 Comparison of numerical and experimental surface and bondline temperature distributions for STS-2, near windside centerline, 80% length: thermocouple measurement 99,761.

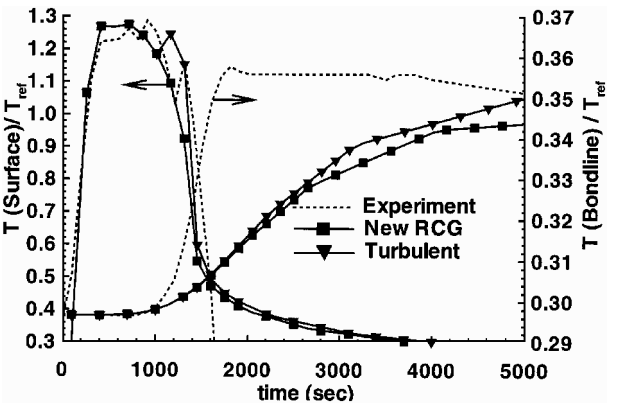

Fig. 25 Comparison of numerical and experimental surface and bondline temperature distributions for STS-2, near wing tip: thermocouple measurement 99,191.

An examination of the numerical and flight surface temperatures in Figs. 15–25 shows that surface temperatures and heat transfer follow similar trends. In regions where the heat transfer is overpredicted or underpredicted, the surface temperatures are overpredicted or underpredicted. Overall, however, the comparison between the numerical and flight surface temperatures is better than the comparison between numerical and flight surface heat transfer. Comparing Figs. 11 and 22, which correspond to the thermocouple on top of the wing, the numerical heat transfer predictions are 2–3 times higher than the flight data in the earlier portion of the trajectory, but the numerical surface temperatures are only about 20–40% greater than the flight data. The better agreement with the temperature data is not unexpected because the heat transfer varies approximately as T^4. Thus, the errors in the heat-transfer comparison are magnified relative to the temperature comparisons. Another observation is that the temperature profiles seem to be smoother than heat-transfer profiles. Comparing Figs. 10 and 21, which are for the thermocouple below the cargo bay hinge line, the jagged nature of the surface heat-transfer profile is not duplicated in the surface temperature profiles and the agreement between the numerical and flight surface temperature profiles is better than for the surface heat transfer.

In this study, the numerical prediction of the maximum surface temperature, which is important for TPS material selection, is good. For the new RCG group, the largest error is at 79,622 (see Fig. 22); the maximum numerical surface temperature overpredicts the maximum flight surface temperature by about 100 K. The second largest error is at 99,341 (see Fig. 15); the maximum numerical surface temperature overpredicts the maximum flight surface temperature by about 50 K. Including the previous two points, the average predicted maximum surface temperature for the new RCG group is within 30 K of flight data.

A comparison of numerical and flight bond-line temperatures is shown in Figs. 15, 16, 19, 20, and 23–25. Although the reference temperature used for the surface and bond-line temperatures is the same, the scale for the bond-line temperature is greatly expanded; the maximum differences in temperatures are about 20 K. The shape and magnitude of the bond-line temperatures do not agree well with the flight data. In general, the peak bond-line temperature is underpredicted. Further, the response time for the bond-line thermocouples is much longer and slower than for the surface thermocouples because of the heat soak, which is the energy that is trapped in the center of the tile during the entry heat pulse. In Fig. 15, the bond-line temperatures are still increasing nearly 1 h after the re-entry heat pulse has ended.

Some of the difference between the numerical and flight data may result from the following factors: multidimensional effects, forced convection, and estimates of the structural thermal mass. In Ref. 27, a multidimensional conduction analysis with the flight data for all of the thermocouples shown in this study is performed; the effects

of flow through the tile gaps and gap heating are included in the study. Nevertheless, the bond-line temperatures are underpredicted. In Ref. 28, the shuttle-tile conduction problem is repeated by a more detailed multidimensional analysis and includes the effects of forced convective cooling. Late in the trajectory, to repressurize the internal compartments in the shuttle, vents are opened that allow cool ambient air to enter the internal structure. This air provides a cooling mechanism that is not modeled in the present work. In Ref. 28, a good numerical prediction of the flight bond-line temperatures is obtained as a result of the improved multidimensional and forced convection modeling. Finally, for a one-dimensional analysis, an estimate of the structural thermal mass is required. This quantity is input into the one-dimensional conduction code as a thickness $\bar{t}$. In general, $\bar{t}$ is set larger than the actual skin thickness at a given surface location because the internal structure acts as a heat sink. In this work, the heat sink provided by the structure is ignored and only the actual structural skin thickness is used. An estimate of $\bar{t}$ requires a detailed multidimensional conduction analysis. Estimates of $\bar{t}$ are available in Ref. 27 for the shuttle, but, for most calculations, this type of information is not readily available. The effect of the added structural mass is to lower the bond-line temperature because the structure acts as a heat sink. The magnitude of the effect is on the order of 5–10 K.

Reviewing the comparisons of the flight and numerical predictions of the bond-line temperatures, it is concluded that the one-dimensional conduction method used in this study is nonconservative relative to the prediction of the bond-line temperatures. The bond-line temperature is usually underpredicted by 20–30 K. This magnitude of error is acceptable for a preliminary design and can be accounted for in the TPS sizing process by using a more conservative bond-line temperature.

Comparisons of TPS Thicknesses

In this final section, the predictions of surface heat transfer and temperature are used to size the TPS at the thermocouple locations. One-dimensional stackups, consisting of LI-900 or LI-2200 tiles on top of Nomex felt (uncoated FRSI) bonded to aluminum, are used. The tile properties, thermal conductivity, heat capacity, and density used for sizing are tabulated in Ref. 20. A maximum bond-line temperature of 450 K is assumed for the aluminum. The TPS thickness is sized under the constraint that the maximum temperature within the aluminum during the 5000-s heat soak is within 1 K of the maximum bond-line temperature. This assumption is nonconservative. For an actual TPS design, margins are always added to account for uncertainties in the sizing methodology. For example, to account for uncertainties related to turbulent transition, a margin could be added directly to the predicted thickness of the TPS, which would reduce the bond-line temperature, or the bond-line temperature used in the sizing could be lowered, which leads to a thicker TPS. In this study, TPS margin analysis, which is always a subject of debate, is not directly addressed. One step in TPS margin analysis, however, is an assessment of the fidelity of the design methodology.

The results of the calculations using the new RCG, old RCG, and turbulent heating profiles are shown in Table 4. The first conclusion derived from the table is that TPS on STS-2 provides a large margin. The thicker tiles, 99,341, 99,201, 99,171, and 99,171, are 2–3 times larger than necessary. The margin increases to a factor of 5 times for some of the thinner tiles, 79,786, 99,337, and 99,761. Further, although the numerical surface heat-transfer profiles are overpredicted by a large margin for the 79,662 tile, the required thickness is almost an order of magnitude too thick. Finally, for the 79,813 and 79,901 tiles, the sizing calculation shows that a tile is not needed; FRSI is an adequate TPS material. Of course, these margins will shrink if an earlier transition criterion is used. The effect of using the old RCG or new RCG kinetics is minimal. As expected, the increase in the heat load from turbulent heating increases the TPS thicknesses. For the windside tiles most affected by turbulence, however, the percentage change in the thickness from turbulence is less than the percentage change in the heat load from turbulence. For example, at 99,761, a 26% change in the total heat load from turbulent heating leads to a 22.5% increase in the TPS thickness. From these sizing calculations, it is concluded that applying a coupled Navier–Stokes and conduction methodology to the TPS design of future RLVs will lead to better TPS mass estimates.

Table 4 Comparison of flight and numerically sized TPS thicknesses

Measurement	Material	Flight, cm	Old RCG, cm	New RCG, cm	Turbulent, cm
99,341	HRSI	8.39	4.16	4.06	4.21
99,337	LRSI	1.66	0.22	0.15	0.28
79,876	HRSI	1.58	0.32	0.32	0.43
79,813	LRSI	0.91	$\ll$0.1	$\ll$0.1	$\ll$0.1
99,381	HRSI	4.35	1.92	1.87	2.12
99,201	HRSI	7.06	2.2	2.17	2.24
79,901	LRSI	1.17	$\ll$0.1	$\ll$0.1	$\ll$0.1
79,622	LRSI	2.09	0.21	0.2	0.26
99,171	HRSI	5.61	1.64	1.60	1.9
99,761	LRSI	2.63	1.14	1.11	1.36
99,191	HRSI	6.51	1.78	1.74	1.95

Concluding Remarks

A validation of the shuttle heating environment has been carried out to assess the applicability of trajectory-based TPS sizing for RLV TPS design. A three-dimensional, chemically reacting Navier–Stokes solver combined with a one-dimensional conduction code are used at eight points along the STS-2 re-entry trajectory to generate 22 flowfield solutions. Quantities necessary for TPS design, surface heat transfer and temperature profiles vs time, integrated heat load, bond-line temperature profiles vs time, and TPS thicknesses are generated and compared with the STS-2 flight data at 11 surface locations. A reasonable comparison with the flight data is observed for the windside locations of the vehicle where the integrated heat loads are largest; these areas account for most of the TPS mass. At three surface locations where the integrated heat loads are small, on top of the wing, on the leeside centerline, and below the cargo bay hinge line, the comparisons are not as good. It was concluded that a better comparison would be obtained with more tangential and streamwise grid resolution. Although, because the impact of the errors on the overall TPS mass are small, the extra grid resolution is probably not necessary for TPS design. In light of the comparison, it is concluded that the trajectory-based TPS sizing methodology used in this study is a beneficial tool for TPS design and an aid in establishing the accuracy and validity of an RLV TPS design database. Further, as computer resources become less expensive and more powerful, the application of the method will become faster, less expensive, and more accurate.

In this study, two curve fits for RCG surface kinetics are compared. Surface heat transfer using a more recent curve fit for RCG is shown to compare slightly better with the flight data. The effects of turbulent heating are considered. In one calculation, fully turbulent flow is assumed about 80 s before it actually occurs during flight. For a number of windside surface locations, the numerical estimates of integrated heat load are increased by 20–25%, assuming early transition. The numerical heat-transfer predictions, assuming fully turbulent flow, agree reasonably well with the flight data at locations where the flow is clearly turbulent. Thus, it is believed that the trajectory-based sizing methodology will provide at least a qualitative estimate of the sensitivity of TPS mass to transition to turbulence.

Finally, the TPS at each surface location is resized by using the numerical heat-transfer predictions and compared with the tile thicknesses used on the flight. The comparisons show that, for STS-2, the TPS margins are quite large, 2–3 times on the windside surfaces, to as high as an order of magnitude on the leeside surfaces. Of course, if transition occurs earlier in the trajectory, which has been observed, then these margins would be significantly reduced. Nevertheless, these comparisons demonstrate the potential for reducing TPS mass by using a high-fidelity, trajectory-based TPS sizing.

Acknowledgments

The authors thank Don Curry at NASA Johnson Space Center for providing the STS-2 bond-line data used in the comparisons. The authors also thank Dave Throckmorton and Vince Zoby of NASA

Langley Research Center for some helpful discussions relative to comparisons with the flight data.

References

[1]Haney, J. W., "Orbiter (Pre STS-1) Aeroheating Design Data Base Development Methodology: Comparison of Wind Tunnel and Flight Test Data," *Orbiter Experiments (OEX) Aerothermodynamics Symposium*, edited by D. A. Throckmorton, Pt. 2, NASA CP-3248, April 1993, pp. 607–676.

[2]Chen, Y.-K., Henline, W. D., Olynick, D. R., and Palmer, G. E., "Three-Dimensional Hypersonic Flowfields and Heating Analysis over the DC-3 Vehicle," AIAA Paper 95-2081, June 1995.

[3]Henline, W. D., Palmer, G. E., Milos, F. S., Olynick, D. R., and Chen, Y.-K., "Aerothermodynamic Heating Analysis and Heatshield Design of an SSTO Rocket Vehicle for Access-to-Space," AIAA Paper 95-2079, June 1995.

[4]Palmer, G. E., Henline, W. D., Olynick, D. R., and Chen, Y.-K., "Heating Analysis of a Lifting Body Single-Stage-to-Orbit Vehicle," AIAA Paper 95-2080, June 1995.

[5]Olynick, D. R., and Henline, W. D., "Aspects of Navier–Stokes Heating Calculations for Benchmark TPS Sizing," *Journal of Spacecraft and Rockets* (to be published).

[6]Hartung, L. C., and Throckmorton, D. A., "Space Shuttle Entry Heating Data Book, Volume I: STS-2," NASA Rept. 1191, Pts. 1 and 2, May 1988.

[7]Gnoffo, P. A., Weilmuenster, K. J., and Alter, S. J., "Multiblock Analysis for Shuttle Orbiter Re-entry Heating from Mach 24 to Mach 12," *Journal of Spacecraft and Rockets*, Vol. 31, No. 3, 1994, pp. 367–377.

[8]Gnoffo, P. A., "An Upwind-Biased Point-Implicit Relaxation Algorithm for Viscous, Compressible Perfect-Gas Flows," NASA TP-2953, Feb. 1990.

[9]Gnoffo, P. A., Gupta R. N., and Shinn, J. L., "Conservation Equations and Physical Models for Hypersonic Air Flows in Thermal and Chemical Nonequilibrium," NASA TP-2867, Feb. 1989.

[10]Walters, R. W., Cinnella, P., and Slack, D. C., "A Status Report on GASP—A General Aerodynamic Simulation Program," *Seventh National Aero-Space Plane Symposium*, NASA Lewis Research Center, 1989 (Paper 9).

[11]McGrory, D. M., Slack, D. C., Applebaum, M. P., and Walters, R. W., "GASP Version 2.2: User's Manual," AeroSoft, Inc., Blacksburg, VA, 1993.

[12]Hirsch, C., *Numerical Computation of Internal and External Flows, Vol. 2: Computation Methods for Inviscid and Viscous Flows*, 1st ed., Wiley, New York, 1990, pp. 493–583.

[13]Park, C., "Review of Chemical-Kinetic Problems of Future NASA Missions, I: Earth Entries," *Journal of Thermophysics and Heat Transfer*, Vol. 7, No. 3, 1993, pp. 385–398.

[14]Wilke, C. R., "A Viscosity Equation for Gas Mixtures," *Journal of Chemical Physics*, Vol. 18, No. 4, 1950, pp. 517–519.

[15]Blottner, F. G., Johnson, M., and Ellis, M., "Chemically Reacting Viscous Flow Program for Multi-Component Gas Mixtures," Sandia Labs., Rept. SC-RR-70-754, Albuquerque, NM, Dec. 1971.

[16]Baldwin, B. S., and Lomax, H., "Thin-Layer Approximation and Algebraic Model for Separated Turbulent Flows," AIAA Paper 78-257, Jan. 1978.

[17]Cleland, J., and Iannetti, F., "Thermal Protection System of the Space Shuttle," NASA CR-4227, June 1989.

[18]Goldstein, H. E., Leiser, D. B., and Katvala, V., "Reaction Cured Borosilicate Glass Coating for Low Density Fibrous Silicia Insulation," *Borate Glass: Structure, Properties, Applications*, Plenum, New York, 1978; also presented at Boron in Glass Ceramics Conf., Alfred Univ., Alfred, NY, June 1977.

[19]Milos, F. S., and Rasky, D. J., "Review of Numerical Procedures for Computational Surface Thermochemistry," *Journal of Thermophysics and Heat Transfer*, Vol. 8, No. 1, 1994, pp. 24–34.

[20]Chiu, S. A., and Pitts, W. C., "Reusable Surface Insulations for Reentry Spacecraft," AIAA Paper 91-0695, Jan. 1991.

[21]Williams, S. D., Curry, D. M., Chao, D., and Pham, V. T., "Analysis of the Shuttle Orbiter Reinforced Carbon-Carbon Oxidation Protection System," NASA TM-104792, June 1994.

[22]Stewart, D. A., Rakich, J. V., and Chen, Y.-K., "Flight Experiment Demonstrating the Effect of Surface Catalysis on the Heating Distribution over the Space Shuttle Heat Shield," *Orbiter Experiments (OEX) Aerothermodynamics Symposium*, edited by D. A. Throckmorton, Pt. 2, NASA CP-3248, April 1993, pp. 677–702.

[23]Stewart, D. A., Pallix, J., and Esfahani, L., "Surface Catalytic Efficiency of Candidate Ceramic Thermal Protection Materials for SSTO," NASA CDTM-20007, March 1995.

[24]Chen, Y.-K., and Milos, F. S., "Solution Strategy for Thermal Response of Nonablating Thermal Protection Systems at Hypersonic Speeds," AIAA Paper 96-0615, Jan. 1996.

[25]Bertin, J. J., Bouslog, S. A., Wang, K. C., and Campbell, C. H., "A Review of Recent Aerothermodynamic Flight Measurements for the Shuttle Orbiter," AIAA Paper 95-0295, Jan. 1995.

[26]Olynick, D., "Importance of 3-D Grid Resolution and Structure for Calculating Reentry Heating Environments," AIAA Paper 96-1857, June 1995.

[27]Norman, I., Rochelle, W. C., Kimbrough, B. S., Ritrivi, C. A., Ting, P. C., and Dotts, R. L., *Comparison of Orbiter STS-2 Development Flight Instrumentation Data with Thermal Math Model Predictions*, edited by P. E. Bauer and H. E. Collicot, Vol. 85, Progress in Astronautics and Aeronautics, AIAA, New York, 1983, pp. 234–254.

[28]Hong, S. I., and Neuenschwander, W. E., "Internal Convective Heat Transfer Mechanism in Reentry Space Vehicles," AIAA Paper 91-1440, June 1991.

J. C. Adams Jr.
Associate Editor